MAL2 mediates the formation of stable HER2 signaling complexes within lipid raft-rich membrane protrusions in breast cancer cells

Jaekwang Jeong[1,8,9,*], **Jae Hun Shin**[1,2,8], **Wenxue Li**[3], **Jun Young Hong**[4], **Jaechul Lim**[2], **Jae Yeon Hwang**[5], **Jean-Ju Chung**[5], **Qin Yan**[6], **Yansheng Liu**[3], **Jungmin Choi**[7], **John Wysolmerski**[1]

[1]Section of Endocrinology and Metabolism, Department of Internal Medicine, Yale University School of Medicine, New Haven, CT 06520, USA

[2]Department of Immunobiology, Yale University School of Medicine, New Haven, CT 06520, USA

[3]Department of Pharmacology, Cancer Biology Institute, Yale University School of Medicine, West Haven, CT 06516, USA

[4]Department of Systems Biology, College of Life Science and Biotechnology, Yonsei University, Seoul, South Korea

[5]Department of Cellular and Molecular Physiology, Yale University School of Medicine, New Haven, CT 06520, USA

[6]Department of Pathology, Yale University School of Medicine, New Haven, CT 06520, USA

[7]Department of Biomedical Sciences, Korea University College of Medicine, Seoul, South Korea

[8]These authors contributed equally

[9]Lead contact

SUMMARY

The lipid raft-resident protein, MAL2, has been implicated as contributing to the pathogenesis of several malignancies, including breast cancer, but the underlying mechanism for its effects on tumorigenesis is unknown. Here, we show that MAL2-mediated lipid raft formation leads to HER2 plasma membrane retention and enhanced HER2 signaling in breast cancer cells. We demonstrate physical interactions between HER2 and MAL2 in lipid rafts using proximity ligation assays. Super-resolution structured illumination microscopy imaging displays the structural

organization of the HER2/Ezrin/NHERF1/PMCA2 protein complex. Formation of this protein complex maintains low intracellular calcium concentrations in the vicinity of the plasma membrane. HER2/MAL2 protein interactions in lipid rafts are enhanced in trastuzumab-resistant breast cancer cells. Our findings suggest that MAL2 is crucial for lipid raft formation, HER2 signaling, and HER2 membrane stability in breast cancer cells, suggesting MAL2 as a potential therapeutic target.

Graphical Abstract
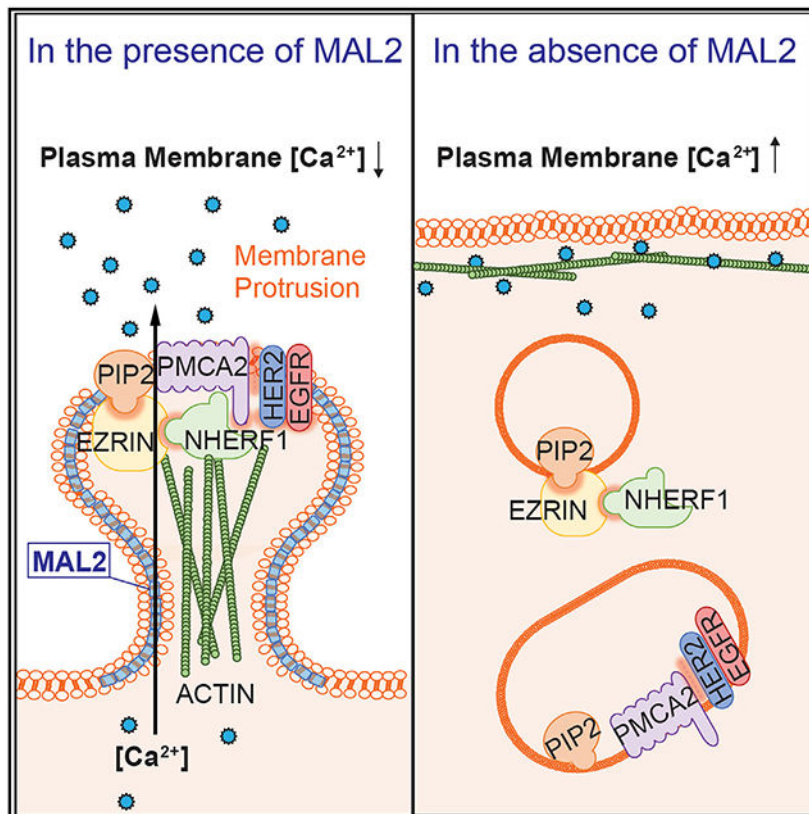
In brief

Jeong et al. show that the formation of MAL2-mediated lipid raft-rich membrane protrusions is crucial for HER2 signaling in breast cancer cells. MAL2 is required for the formation of HER2/ Ezrin/NHERF1/PMCA2 protein complexes. Formation of these protein complexes leads to a low calcium environment in the plasma membrane

INTRODUCTION

Approximately 20% of invasive breast cancers overexpress the receptor tyrosine kinase, ERBB2/HER2/Neu (HER2), most commonly due to amplification of the *ERBB2* gene. In breast and other cancers, HER2 overexpression predicts more aggressive tumor behavior and increased mortality (Arteaga and Engelman, 2014; Arteaga et al., 2011; Hynes and MacDonald, 2009). HER2 overexpression in MMTV-Neu transgenic mice is sufficient

to cause breast tumors, demonstrating its direct oncogenic activity (Guy et al., 1992; Hanker et al., 2013). HER2 has no known ligands and acts as an obligate heterodimer, partnering with other members of the ErbB receptor family, especially with ERBB1/EGFR and ERBB3/HER3 in breast cancers (Olayioye, 2001). Unlike other ERBB family members, HER2 resists internalization and degradation upon activation, remaining on the cell surface and/or being rapidly recycled to the plasma membrane. HER2 also impedes the endocytosis and degradation of its heterodimerization partners, EGFR and HER3. The mechanisms underlying the membrane retention of activated HER2 are only partly understood, but this property correlates with the localization of HER2 within discrete protruding membrane domains and requires interactions with HSP90 (Bertelsen and Stang, 2014; Li et al., 2020). In addition, our studies have recently demonstrated that interactions of HER2 with the calcium pump, PMCA2, and two scaffolding molecules, NHERF1 and Ezrin, are important to support the localization of HER2 within lipid raft-rich membrane protrusions, the interactions between HER2 and HSP90, the retention of activated HER2 on the cell surface, and downstream HER2 biochemical signaling (Jeong et al., 2016, 2017b, 2018).

Lipid rafts are cholesterol- and sphingolipid-rich membrane microdomains that regulate cellular functions, such as membrane trafficking, receptor signaling, and the organization of apical membrane microvilli (Alonso and Millan, 2001; Lajoie and Nabi, 2010; Patel and Insel, 2009; Pike, 2003, 2005; Schuck and Simons, 2004; Simons and Sampaio, 2011). In cancer cells, lipid rafts sequester and concentrate oncogenic signaling components and, thus, contribute to malignant transformation or behavior (Li et al., 2006; Mollinedo and Gajate, 2015; Staubach and Hanisch, 2011). Structurally, lipid raft domains are more rigid and tightly packed portions of the membrane that are resistant to solubilization with certain detergents such as Triton X-100 (Brown, 2006; Schuck et al., 2003). We and others have reported that HER2, along with PMCA2, NHERF1, and Ezrin, is located within lipid raft-rich portions of the membrane (Jeong et al., 2016, 2017b, 2018; Nagy et al., 2002).

MAL2 is a resident protein of lipid rafts, and is known to function in apical trafficking (de Marco et al., 2002; Schuck and Simons, 2004). The *MAL2* gene is expressed in various tumor tissues, including breast cancers, and increased levels of MAL2 in tumor cells are associated with a reduction in survival (Bhandari et al., 2018; Li et al., 2017; Shehata et al., 2008). However, little is known about the functions of MAL2 in tumor cells. In this report, we present evidence that MAL2 supports HER2 localization and function. Our data suggest that MAL2 is important for concentration and clustering of HER2 within specific lipid raft-containing membrane microdomains, bringing together the scaffolding and signaling molecules required for HER2 signaling and membrane retention.

RESULTS

Correlation of lipid raft-rich membrane protrusions with HER2 expression

We observed colocalization of HER2 and fluorescently labeled cholera toxin B (CTB), a marker of lipid raft domains, in the plasma membrane of HER2-positive SKBR3 breast cancer cells (Figure 1A, lower). Plasma membrane CTB fluorescence intensity was less in immortalized but non-transformed human MCF10A epithelial cells than it was in SKBR3 breast cancer cells, as was the quantification of lipid raft area as determined by CTB staining

(Figures 1A and 1B). Knocking down HER2 expression with small hairpin RNA (shRNA) and inhibiting HER2 signaling with lapatinib reduced lipid raft areas in SKBR3 cells, suggesting a relationship between HER2 expression/signaling and the formation of lipid rafts (Figure 1B). In support of this idea, the gene expression of lipid raft-resident proteins, such as Flotillin 1 (FLOT1), MAL, and MAL2, was increased in SKBR3 and/or BT474, HER2-positive breast cancer cells as compared with MCF10A cells (Figure 1C) (Asp et al., 2014; Pust et al., 2013). We obtained similar results when we examined the expression of these genes in breast tumors in The Cancer Genome Atlas (TCGA) database; *FLOT1* and *MAL2* mRNA levels were increased in HER2-positive breast cancers (Figure 1D) as compared with normal breast tissue. In addition, single-cell RNA sequencing (scRNA-seq) of tumor samples from breast cancer patients demonstrated co-expression of HER2 with Flotillin and especially with MAL2 within specific cell clusters (Figures 1E and 1F) (Chung et al., 2017). In addition, scRNA-seq of tumor and immune cells from breast cancer patients identified a HER2-positive cell population (cluster 2) where co-expression of MAL2 with HER2 occurred in 95.9% of HER2-positive cells as compared with co-expression of Flotillin with HER2, which occurred in 49.3% of HER2-positive cells (Figures 1E and S1A) (Chung et al., 2017). Expression of MAL2 in HER2-positive cells was significantly higher than both MAL and FLOT1 (Figure 1F), consistent with the presence of stronger ATAC-seq peaks within the promoter region of MAL2 as compared with MAL and FLOT1 in SKBR3 cell lines (Figures 1G and S1B).

We observed that HER2 colocalized with MAL2 in portions of the plasma membrane that also stained for CTB, suggesting they interacted within lipid raft-rich protrusions (Figure 2A). As expected, in MCF10A cells, which have low HER2 and MAL2 mRNA levels, there was no staining for HER2 and faint immunofluorescence for MAL2, which did not appear to be localized at the plasma membrane (Figure S2A). We further validated direct interactions between MAL2 and HER2 by overexpressing FLAG-tagged MAL2 in SKBR3 cells and by performing co-immunofluorescence and proximity ligation assays to detect MAL2 and HER2 interactions. As shown in Figure 2B, staining for the FLAG tag colocalized with staining for HER2 and actin (phalloidin) in membrane protrusions from SKBR3 cells. Similarly, we detected positive proximity ligation assay (PLA) signals for interactions between MAL2 and HER2 in SKBR3 cells, and the positive signals colocalized with fluorescent phalloidin staining to detect actin expression in membrane protrusions (Figure 2C). These interactions were dependent on lipid raft formation, as depleting membrane cholesterol using methyl-β-cyclodextrin (MβCD) greatly reduced co-immunofluorescence and PLA signals for HER2 and MAL2 (Figures 2B and 2C). Furthermore, MβCD treatment inhibited the formation of membrane protrusions and caused cytosolic accumulation of HER2 and MAL2 (Figures 2B and 2C).

MAL2 expression is required for the formation of membrane protrusions

Next, we generated stable MAL2-knockdown SKBR3 and BT474 cells (MAL2KD_SKBR3, MAL2KD_BT474), and achieved approximately 60% reduction of MAL2 mRNA levels in both cell lines (Figure 2D). Knocking down MAL2 inhibited HER2 signaling as demonstrated by reduced levels of total HER2 protein as well as reduced phosphorylation of HER2 and EGFR, although the reduction of pHER2 was greater in MAL2KD_ SKBR3 cells

than in MAL2KD_BT474 cells (Figure 2E). Knocking down MAL2 reduced proliferation in both cell lines, as measured by BrdU incorporation (Figure 2F). As expected, reducing the expression of MAL2 inhibited interactions between HER2 and MAL2 protein measured by PLA (Figure 2G). It also inhibited the formation of lipid raft-rich membrane protrusions. Transmission electron microscopy showed a reduction in complex membrane protrusions in MAL2KD_SKBR3 cells compared with the control cells (Figure 2H). In addition, while HER2 and CTB colocalized within protruding membrane structures in control cells, knocking down MAL2 reduced the intensity of HER2 and CTB fluorescence overall, and staining for both became more diffusely distributed within the plasma membrane as opposed to the punctate pattern of staining in membrane protrusions in control cells (Figure 2I). Similar findings were seen when lipid rafts were disrupted using MβCD, although this also caused internalization of HER2 and CTB fluorescence (Figure 2I).

Another important constituent of lipid rafts is FLOT1, which is co-expressed with MAL2 and associates with HER2 (Gomes et al., 2019; Lin et al., 2011; Ou et al., 2017; Pust et al., 2013). In MAL2KD_SKBR3 and MAL2KD_BT474 cells, FLOT1 mRNA and protein expression were decreased (Figures S2B and S2C). Knocking down MAL2 also impaired the ability FLOT1 to colocalize with HER2. As shown in Figure 2J, when we overexpressed FLAG-tagged FLOT1 in control SKBR3 cells, it colocalized with HER2 within actin-rich, plasma membrane protrusions as expected. However, when we expressed FLAG-tagged FLOT1 in MAL2KD_SKBR3 cells or in SKBR3 cells treated with MβCD, FLOT1 no longer trafficked to the membrane, no longer colocalized with HER2 and, instead, accumulated in the cytoplasm (Figure 2J).

We previously found that the formation of lipid raft-rich membrane protrusions depends on HER2 signaling (Jeong et al., 2017a). Given that the expression of both MAL2 and FLOT1 was increased in HER2-positive breast cancer cells (Figure 1), we also examined whether inhibiting HER2 expression would affect MAL2 and FLOT1 expression and/or localization. As shown in Figures S2D-S2F, knocking down HER2 expression decreased the levels of both MAL2 and FLOT1 mRNA. In addition, when we expressed FLAG-tagged MAL2 or FLAG-tagged FLOT1 in HER2KD_SKBR3 cells, we observed that loss of HER2 expression inhibited trafficking of both to the plasma membrane (Figures S2F). Thus, in breast cancer cell lines, HER2 activation regulates the expression and localization of MAL2 and FLOT1, both of which are important to the organization of lipid rafts.

Previous studies have revealed that the loss of membrane protrusions is associated with abnormal internalization and degradation of HER2, especially in response to EGF treatment (Jeong et al., 2016, 2017b, 2018). As expected, in control cells treated with EGF, HER2 remained localized in the plasma membrane, whereas most of the EGFR not associated with HER2 was internalized into the cytoplasm (Figures 2J and 2K, upper). However, after knocking down MAL2, EGF treatment led to internalization of both HER2 and EGFR into the cytoplasm, where they continued to colocalize by immunofluorescence (Figure 2K). PLA experiments confirmed that protein-protein interactions occurred between HER2 and EGFR in the membrane protrusions of control SKBR3 cells (Figure 2L, upper). These interactions were not disrupted upon HER2 internalization in MAL2KD_SKBR3 cells, but the PLA signal indicating interactions between HER2 and EGFR occurred within the

cytoplasm and not at the membrane (Figure 2L, lower). In addition, the colocalization of HER2/EGFR heterodimers with phalloidin was significantly reduced (Figures 2L and 2M). These data suggest that MAL2 expression is necessary for the retention of HER2-EGFR complexes at the cell surface within actin-rich membrane protrusions, but not for the ability of HER2 and EGFR to interact.

Loss of lipid rafts disrupts the HER2/Ezrin/NHERF1 protein complex

Interactions with Ezrin and NHERF1 are important for retention of HER2 within actin and lipid raft-enriched domains at the cell surface (Jeong et al., 2017b, 2018). Therefore, we examined Ezrin and NHERF1 expression in MAL2KD_SKBR3 cells as well as in SKBR3 cells treated with MβCD, since both manipulations reduced the formation of lipid rafts and membrane protrusions. We found a 50% reduction of NHERF1 mRNA expression in MAL2KD_SKBR3 cells but no change in MβCD-treated SKBR3 cells (Figure S3A). In contrast, Ezrin expression was unchanged in MAL2KD_SKBR3 cells and actually increased by 50% in MβCD-treated SKBR3 cells (Figure S3A). Regardless of the variable changes in gene expression, knockdown of MAL2 and MβCD treatment both disrupted the typical pattern of immunofluorescence colocalization of HER2 with Ezrin or NHERF1 within protrusions and resulted in accumulation of HER2 within the cytoplasm (Figures S3B and S3C).

To better understand the structural organization of the HER2/Ezrin/NHERF1 protein complex as well as its reliance on MAL2, we performed super-resolution, structured illumination microscopy (SIM imaging) in control SKBR3 cells and in MAL2KD_SKBR3 cells. The HER2/Ezrin/NHERF1 protein complex was mainly detected in a convex outcropping of the plasma membrane in control cells, with actin located at the base and central core of these protrusions, while HER2 was concentrated more at the surface and distal aspects of the structures. Ezrin and NHERF1 colocalized with both actin and HER2 and often appeared to bridge the actin core and membrane HER2 (Figures 3A, 3B, S4A, and S4B). We observed less direct colocalization between HER2 and actin. The formation of membrane protrusions was disrupted in MAL2 knockdown and MβCD-treated SKBR3 cells (Figures 3C, 3D, S4C, S4D, and S5). Loss of these structures was associated with a rearrangement of the actin into rod-like structures often at the periphery of individual cells. There was also a significant reduction of the interactions between Ezrin and NHERF1 with the actin cytoskeleton as well as variable reduction with their interaction with HER2. Areas of interaction between HER2 with NHERF1 and/or Ezrin appeared to be smaller in size and occurred within the cytoplasm rather than exclusively on the cell surface (Figures 3C, 3D, S4C, and S4D). Similar results were noted when cells were treated with MβCD (Figure S5).

Next, we tested protein-protein interactions among these same molecules using PLA. Approximately 40% of control cells demonstrated strong PLA signals signifying direct interactions between HER2 and Ezrin or HER2 and NHERF1 concentrated within membrane protrusions and colocalizing with actin as detected by phalloidin staining (Figures 3E and 3F). In contrast, MAL2 knockdown and MβCD-treated SKBR3 cells showed a significant overall reduction in PLA fluorescence for interactions between HER2 and Ezrin or HER2 and NHERF1 as well as dramatic reductions in PLA signals in plasma

membrane protrusions (Figures 3F and 3G). In addition, the residual HER2/NHERF1 PLA signals shifted from the membrane into the cytoplasm (Figure 3E). These differences were also observed when control and MAL2KD_SKBR3 cells were acutely treated with EGF. Consistent with previous results, EGF treatment results in more prominent interactions between HER2 and Ezrin or NHERF1 within membrane protrusions in control cells. However, knockdown of MAL2 results in less prominent interactions at the membrane and a shift toward PLA interactions present in the cytoplasm (Figures S6A and S6B).

Lipid raft-rich membrane protrusions concentrate phosphatidylinositol 4,5-bisphosphate to form the HER2/Ezrin/actin cytoskeleton protein complex

Activated Ezrin interacts with both the actin cytoskeleton and phosphatidylinositol 4,5-bisphosphate (PIP2) at the inner aspect of the plasma membrane (Bosk et al., 2011; Janke et al., 2008; Jayasundar et al., 2012). Given that our previous studies showed enrichment of PIP2 within membrane protrusions, we expressed the pleckstrin homology domain of phospholipase C-delta fused to green fluorescent protein (PH-PLCδ-GFP) to monitor local concentrations of PIP2 on the plasma membrane within control and MAL2_KD SKBR3 cell lines. As expected, PH-PLCδ-GFP was enriched together with Ezrin and HER2 in a punctate pattern within actin-containing membrane protrusions in control SKBR3 cells (Figure 4A). Knocking down MAL2 or treating cells with MβCD caused the redistribution of PH-PLCδ-GFP more generally throughout the plasma membrane as well as its accumulation in the cytoplasm, where it colocalized with HER2 but not with Ezrin (Figures 4B and 4C). These results suggest that MAL2 expression is required for the concentration of PIP2 within membrane protrusions as well as the binding of phosphorylated Ezrin to PIP2 and its association with HER2.

In addition to anchoring Ezrin to the plasma membrane, PIP2 is a substrate for phosphoinositide 3-kinase (PI3K), an important signaling molecule downstream of HER2 activation. Ezrin has been shown to affect PI3K/Akt activity and, conversely, Ezrin phosphorylation/activation can be regulated by PI3K (Elliott et al., 2005; Quan et al., 2019). Therefore, we also examined the effects of the PI3K inhibitor, wortmannin, on interactions between HER2, Ezrin, and PIP2 in membrane protrusions. In the presence of 10 μM of wortmannin, PH-PLCδ-GFP accumulated in the cytoplasm, where it continued to colocalize with HER2 but not with Ezrin (Figures 4D and 4E). These results were consistent with MAL2 knockdown and MβCD treatment (Figures 4A-4C). Co-immunostaining and PLA confirmed that wortmannin treatment disrupted interactions between HER2 and Ezrin (Figures 4F and S7A). Wortmannin treatment also reduced the phosphorylation of Ezrin (Figures S7B). Interestingly, Ezrin phosphorylation and the PLA signal between Ezrin and HER2 were more sensitive to lower doses of wortmannin than was colocalization of Ezrin and HER2 by immunofluorescence, which was disrupted only at 10 μM wortmannin. These results suggest that reduced Ezrin phosphorylation may cause HER2 and Ezrin. to dissociate before inhibition of PI3K leads to remodeling of membrane protrusions.

PI3K phosphorylates AKT, which acts as an important downstream mediator of the oncogenic activity of HER2. Therefore, we also tested the levels and localization of phosphorylated AKT (pAKT) in MAL2_KD SKBR3 cells and in SKBR3 cells treated with

MβCD. As shown in Figure 4G, neither reductions in MAL2 expression nor disruption of lipid rafts reduced total AKT or pAKT levels. However, these manipulations changed the cellular location of pAKT. As observed by 3D SIM imaging, in control cells, pAKT was enriched within membrane protrusions where it closely overlapped with HER2 staining (Figure 4H). In contrast, in MAL2 knockdown or MβCD-treated SKBR3 cells, pAKT localized within the cytoplasm of the cells, and no longer overlapped with HER2 staining (Figures 4I and 4J). This alteration in pAKT localization correlated with persistence of nuclear FOXO1 and a reduction in cell viability in MAL2 knockdown or MβCD-treated SKBR3 and BT474 cells, suggesting a reduction in the biological activity of pAKT (Figures 4K and 4L). These results demonstrate the close structural and functional interactions between PIP2, Ezrin, HER2, and PI3K/pAKT within membrane protrusions that, in turn, rely on MAL2 and lipid raft content for their organization.

Lipid raft-rich membrane protrusions maintain low intracellular calcium levels

Elevated cellular calcium levels can inhibit activation of HER2 signaling and disrupt membrane protrusions (Jeong et al., 2016, 2017a). Therefore, we utilized Lck-GCaMP5G, consisting of the genetically encoded calcium sensor GCaMP5G fused to the 26 amino acid, membrane targeting sequence of Src tyrosine kinase (Lck), to monitor intracellular calcium levels near the plasma membrane (Akerboom et al., 2012; Shigetomi et al., 2010). Membrane fluorescence from Lck-GCaMP5G was low in control SKBR3 cells but increased significantly in response to treatment with ionomycin and extracellular calcium, disruption of MAL2 (MAL2_KD cells), or treatment with MβCD (Figures 5A-5C). PMCA2 maintains low intracellular calcium levels, is co-expressed with HER2 in membrane protrusions, and is required for HER2 membrane retention and signaling (Jeong et al., 2016). Given the increase in calcium levels at the plasma membrane in MAL2_KD cells and in cells treated with MβCD, we also examined the expression and localization of PMCA2. PMCA2 protein levels were unchanged in MAL2_KD cells as well as in response to MβCD treatment, even though mRNA levels were significantly increased in both conditions (Figures 5D and 5E). We next tested direct protein-protein interactions between HER2 and PMCA2. Consistent with our previous reports, both endogenous and overexpressed GFP-tagged PMCA2 interacted closely with HER2 in the membrane protrusions (Figures 5F-5H) (Jeong et al., 2016). However, interactions between PMCA2 and HER2, as detected by PLA, were dramatically reduced in MAL2_KD- and MβCD-treated SKBR3 cells (Figures 5F-5H). SIM imaging analysis showed prominent colocalization of PMCA2 and HER2 within the membrane protrusions (Figure 5I). This colocalization was mostly dissociated in MAL2_KD- and MβCD-treated SKBR3 cells, and PMCA2 was redistributed away from the membrane and into the cytoplasm, especially with MβCD treatment (Figure 5I). The presence of PMCA2 at the membrane helps protect SKBR3 and other breast cancer cells from cell death in response to extracellular calcium and ionomycin (Jeong et al., 2016). Knocking down MAL2 increases apoptosis of SKBR3 cells, both at baseline and in response to calcium and ionomycin treatment (Figure 5J), consistent with the loss of membrane PMCA2 localization. Collectively, these results demonstrate that MAL2 and lipid rafts are required for interactions between PMCA2 and HER2 that, in turn, maintain low calcium concentrations within the vicinity of HER2 membrane signaling complexes.

Interactions of HER2 with MAL2, Ezrin, NHERF1, and PMCA2 are increased in trastuzumab-resistant SKBR3 cells

The humanized anti-HER2 monoclonal antibody, trastuzumab, is commonly used to treat HER2-positive cancers (Arteaga and Engelman, 2014; Gale et al., 2020). Trastuzumab induces HER2 internalization, ubiquitination, and degradation, blocking downstream signaling (Arteaga and Engelman, 2014; Cuello et al., 2001; Escriva-de-Romani et al., 2018; Klapper et al., 2000). There is a significant rate of primary resistance to trastuzumab as well as the frequent emergence of acquired resistance. Although several mechanisms are associated with trastuzumab resistance, resistant cells often demonstrate reduced internalization and degradation of HER2 in response to drug (Arteaga and Engelman, 2014; Barok et al., 2014; de Melo Gagliato et al., 2016; Derakhshani et al., 2020; Escriva-de-Romani et al., 2018; Gale et al., 2020; Vernieri et al., 2019). Because our data demonstrate that MAL2 contributes to the localization of HER2 within lipid raft-rich, membrane protrusions as well as the retention of HER2 at the cell surface, we compared the expression of MAL2 and other constituents of the HER2 signaling complex in control SKBR3 cells versus SKBR3 cells induced to acquire resistance to trastuzumab (Gale et al., 2020). Similar to normal SKBR3 cells, trastuzumab-resistant SKBR3 cells displayed lipid raft-rich plasma membrane protrusions and HER2 colocalized with MAL2 within these structures (Figure 6A and 6B). Using PLA, we found a significant increase in HER2/MAL2 interactions in trastuzumab-resistant cells compared with control cells (Figure 6C). We validated this finding by performing quantitative data-independent acquisition (DIA) mass spectrometry on HER2 immunoprecipitated from both control and resistant SKBR3 cells. These data confirmed that MAL2 interacts with HER2 and that this interaction is enhanced about 2.5-fold in the trastuzumab-resistant cells compared with controls even though HER2 peptide levels, themselves, were no different in resistant cells (Figures 6D-6F). Although mRNA levels for MAL2, Ezrin, and NHERF1 were not different in the trastuzumab-resistant versus trastuzumab-sensitive cells (Figure 6G), PLA demonstrated increased interactions between HER2 and MAL2, HER2 and Ezrin, HER2 and NHERF1, and HER2 and PMCA2 in trastuzumab-resistant cells (Figures 6A, 6H, and 6I). Another important component of the complex stabilizing HER2 at the plasma membrane is HSP90 and physical interactions between HER2 and HSP90 were enhanced in trastuzumab-resistant cells as assessed by PLA and coimmunoprecipitation (Figures 6J and 6K).

We next knocked down MAL2 expression in SKBR3 and BT474 that had previously been established as models of acquired trastuzumab resistance (Gale et al., 2020) as well as in a HER2-positive breast cancer cell line with intrinsic resistance to trastuzumab (JIMT1) (Koninki et al., 2010; Tanner et al., 2004). By definition, trastuzumab did not affect the growth of control cells. In contrast, knocking down MAL2 in trastuzumab-resistant SKBR3 or BT474 cells led to a marked decrease in cell viability in the presence of trastuzumab (Figure 6L). Treating both cell lines with MβCD and trastuzumab had an even greater effect on cell viability. This was accompanied by increased nuclear immunofluorescence for FOXO1 in the resistant cells as well as the redistribution of pAKT away from a punctate pattern of colocalization with HER2 in membrane protrusions to a more diffuse intracellular localization that was no longer colocalized with HER2 (Figures 6M and 6N). In contrast to these results, knocking down MAL2 had no effect on cell viability in JIMT1 cells (Figure

S8A). JIMT1 cells have much lower levels of expression of HER2, MAL2, and FLOT1 than SKBR3 cells (Figure S8B), and HER2 is expressed more diffusely in the membrane without being concentrated in actin-rich membrane domains (Figure S8C). Together, these data suggest that acquired trastuzumab resistance in cells with high levels of HER2 expression is associated with an increase in the interactions between HER2 and MAL2 that also leads to increased interactions of HER2 with Ezrin, NHERF1, PMCA2, and HSP90, all in lipid rafts within membrane protrusions. Reductions in MAL2 expression or disruptions in lipid rafts impair the growth of these cells, recovering their sensitivity to trastuzumab.

DISCUSSION

In this report, we demonstrate correlations between the expression of the lipid raft-associated, apical transport protein, MAL2, and the receptor tyrosine kinase, ErbB2/HER2, in breast cancer cell lines as well as in human breast cancers. Furthermore, using a combination of PLAs, confocal microscopy, and high-resolution SIM imaging, we demonstrate close physical proximity between HER2, MAL2, PMCA2, NHERF1, and Ezrin within lipid raft-rich membrane protrusions. Loss of function studies using MAL2 knockdown cells demonstrate that MAL2 is required for the clustering of HER2/PMCA2/Ezrin/NHERF1 complexes within raft domains as well as the maintenance of a low calcium and PIP2-enriched microenvironment that allows for HER2 membrane retention and HER2/PI3K/Akt signaling. The function of MAL2 within this complex appears to be, at least in part, the maintenance of lipid rafts, as depletion of membrane cholesterol using MβCD mimics most of the effects of knocking down expression of MAL2. Thus, we propose that, in HER2-positive cancer cells, MAL2 is critical for integrating membrane structure, membrane HER2 retention and HER2 biochemical signaling by fostering the clustering of key scaffolding proteins and HER2 signaling components within lipid rafts.

Lipid rafts are cholesterol- and sphingolipid-enriched membrane domains that can serve as platforms clustering a variety of receptor tyrosine kinases (RTKs) and their downstream signaling partners, including both HER2 and EGFR as well as PI3K and Akt (Mollinedo and Gajate, 2015). They support ErbB family homo- and heterodimerization, intensify ErbB biochemical signaling and contribute to cellular transformation (Staubach and Hanisch, 2011). In HER2-positive breast cancer cells, activated HER2 (pHER2) localizes primarily to lipid raft domains, and pharmacological disruption of lipid rafts has been shown to inhibit HER2 signaling as well as to slow proliferation and trigger apoptosis (Alawin et al., 2016). This may be related to the ability of lipid rafts to aggregate proteins, such as caveolins, flotillins, ERM proteins, NHERF1, PMCA2, and HSP90, all of which have been reported to modulate HER2 localization, trafficking, and/or signaling (Jeong et al., 2016, 2017b; Pereira et al., 2018; Pust et al., 2013; Quan et al., 2019). The data presented here demonstrate that MAL2 is another important constituent of lipid rafts necessary for maintaining HER2 signaling in breast cancer cells. MAL2 interacts closely with HER2 within lipid rafts as detected by PLAs and this interaction was greatly diminished by depleting membrane cholesterol with MβCD. Knocking down MAL2 reduced total HER2, pHER2, and pEGFR levels. It also caused abnormal internalization of HER2 together with EGFR in response to receptor activation but did not cause dissociation of the two receptors from each other based on PLAs. Finally, it led to effacement of membrane protrusions normally seen in SKBR3

cells and redistribution of actin away from the apical aspect of the cells to the periphery and basolateral aspect of these cells.

MAL2 is a member of the tetraspanin family of membrane structural proteins that functions in raft-associated membrane trafficking during transcytosis and in the indirect cargo pathway of basolateral to apical vesicle transport (de Marco et al., 2002; Marazuela and Alonso, 2004). A related molecule, MAL1, has been described to facilitate the aggregation of smaller lipid rafts into larger raft domains through self-oligomerization (Magal et al., 2009). The aggregation of smaller rafts into larger complexes has been noted in cancer cells and is thought to be a mechanism by which larger RTK signaling platforms can amplify oncogenic signals (Mollinedo and Gajate, 2020). Although a raft clustering function has not been formally demonstrated for MAL2, our results are consistent with it assembling a multi-protein HER2 signaling complex that includes HER2, Ezrin, NHERF1, PMCA2, and actin. PLAs suggest that knocking down MAL2 reduces but does not completely ablate the interactions of HER2 with these individual components of the signaling complex. Instead, loss of MAL2 causes a redistribution of the interacting proteins more broadly throughout the membrane and prevents their clustering within specific domains. Interestingly, other members of the tetraspanin family are involved in the bending of membranes to form protruding structures (Hemler, 2003). Although neither MAL or MAL2 have been demonstrated to participate in protrusions per se, the loss of such plasma membrane structures in MAL2-knockdown SKBR3 cells suggests that, either directly or indirectly, MAL2 may also facilitate bends in the plasma membrane required for the formation of protrusions.

Our previous work has documented interactions between PMCA2, Ezrin, NHERF1, and HER2 that are required to maintain activated HER2/EGFR and HER2/HER3 heterodimers on the cell surface. In this study, we made use of both co-registration of PLAs with immunofluorescence as well as high-resolution SIM imaging to better resolve the interactions of HER2 with these different proteins. Our results suggest that most of the HER2 in SKBR3 cells is located at the tips of convex protrusions of the apical surface of the cell. These structures have a central actin core oriented perpendicular to the plane of the plasma membrane, surrounded by the scaffolding proteins Ezrin and NHERF1 (Figure 6O). HER2 is located toward the tip of the protrusion and does not colocalize with actin. However, NHERF1 and Ezrin do colocalize with phalloidin staining, consistent with their known functions of linking membrane proteins to the actin cytoskeleton. 3D SR-SIM imaging also documented interaction between HER2 and the calcium pump, PMCA2, toward the more basal reaches of HER2 fluorescence within the protrusions. Furthermore, live cell calcium imaging demonstrated that this organization was associated with low baseline levels of intracellular calcium near the plasma membrane, which is important given that calcium-induced activation of protein kinase C-alpha causes the internalization of HER2 and its degradation (Jeong et al., 2018).

Trastuzumab is the most commonly used targeted agent for HER2-positive cancers (Arteaga and Engelman, 2014; Gale et al., 2020). However, breast cancer cells frequently acquire resistance to this drug through mechanisms not fully understood. We hypothesized that increased interactions between MAL2 and HER2 might contribute to trastuzumab resistance.

Using DIA proteomic and PLA analyses, we confirmed increased physical interactions between HER2 and MAL2 in resistant SKBR3 cells, as well as between HER2 with Ezrin, NHERF1, PMCA2, and HSP90. Importantly, targeting MAL2 levels resensitized resistant cells to trastuzumab resulting in the internalization of HER2, the disruption of Akt signaling, and decreased viability in both resistant SKBR3 and resistant BT474 cells. Much more work will be required to understand the mechanisms that upregulate these protein-protein interactions, but these results suggest that targeting MAL2 may be useful in overcoming or preventing trastuzumab resistance.

In summary, the results presented in this article demonstrate the importance of MAL2 to HER2 localization and signaling within breast cancer cells. We find that MAL2 expression is up-regulated in HER2-positive breast cancers, that MAL2 physically interacts with HER2, and that MAL2 is necessary for HER2 signaling. Our data suggest that MAL2 may play an important architectural role in the aggregation of lipid raft domains and their associated proteins into specialized HER2 signaling domains that contribute to the persistence of activated HER2 on the plasma membrane. Targeting MAL2 and/or its interactions with the HER2 signaling complex may improve the current anti-HER2 therapies.

Limitations of the study

We analyzed increased expression of MAL2 in breast cancer cells using TCGA and patient-derived scRNA-seq data. Our study showed that MAL2 is critical for HER2 membrane retention and signaling in breast cancer cell lines *in vitro.* Therefore, it would be beneficial to confirm our findings using patient-derived primary cells and/or *in vivo* model systems.

STAR★METHODS

RESOURCE AVAILABILITY

Lead contact—Further requests for resources should be directed to and will be fulfilled by the lead contact, Jaekwang Jeong (jaekwang.jeong@yale.edu).

Materials availability—This study did not generate new materials.

Data and code availability

- Data reported in this paper will be shared by the lead contact upon request.

- The accession number for the ATAC-sequencing data reported in this study is GEO: GSE188513.

- Any additional information required for reanalyze the data reported in this paper is available from the lead contact upon request.

METHOD DETAILS

Cell culture—The human cell lines, SKBR3 and BT474 were obtained from ATCC and maintained in culture in DMEM + GlutaMAX-1 (Gibco-life Technologies) containing 10% fetal bovine serum (FBS) and pen/strep (Gibco-life Technologies) at 37°C in 5% CO_2. In some experiments, cells were cultured as above but in media without FBS for 16 hours and

then were treated with 100ng/ml EGF (Cell Signaling) for 2 hours. In other experiments, various pharmacologic agents were added to media; these included MβCD at 5mM for 4 hours before harvesting cells, wortmannin at 2.5μM, 5μM, 10μM, 20μM for 16 hours before harvesting cells. To raise intracellular calcium levels, cells were exposed to 10μM extracellular calcium and 1μM ionomycin.

Trastuzumab resistant SKBR3 and BT474 cell lines were developed in the laboratory of Qin Yan. Baseline SKBR3 and BT474 cells were acquired from ATCC and were exposed to increasing doses of trastuzumab over a 3-month period and the surviving cells were pooled, expanded and maintained in the presence of 10μg/ml dose trastuzumab. JIMT1 cells were developed from a pleural effusion taken from a patient with HER2-positive breast cancer that displayed intrinsic resistance to trastuzumab. They were a kind gift of Dr. Faye Rogers at Yale.

RNA EXTRACTION AND REAL-TIME RT-PCR

RNA was isolated using TRIzol (Invitrogen). Quantitative RT-PCR was performed with the SuperScript III Platinum One-Step qRT-PCR Kit (Invitrogen) using a Step One Plus Real-Time PCR System (Applied Biosystems) and the following TaqMan primer sets: flotillin1, Hs00195134_m1; MAL, Hs00707014_s1; MAL2, Hs01043579_u1; PMCA2, Hs01090447_m1; Ezrin, Hs00931646_m1; NHERF1, Hs00188594_m1. Human HPRT1 (4326321E) (Invitrogen) was used as a reference gene. Relative mRNA expression was determined using the Step One Software v2.2.2 (Applied Biosystems).

Cell transfections—Constructs encoding flag-flotillin1 (RC200231) and flag-MAL2 (RC203862) are commercially available from OriGene (Rockville, MD). GFP-C1-PLCδ-PH (21179), and pN1-Lck-GCaMP5G (34924) are commercially available from Addgene (Cambridge, MA). HA-NHERF1 was gifted from Peter Friedman at University of Pittsburgh. SKBR3 cells were transfected using Fugene6 transfection reagent (Invitrogen) according to the manufacturer"s instructions.

Knockdown cell line—A stable cell line expressing shRNA directed against MAL2 was generated by transducing cells with commercially prepared lentiviruses containing 3 individual shRNA directed against MAL2 mRNA: MAL2 (sc-77560-V) (Santa Cruz). Briefly, cells were cultured in 12-well plates and infected by adding the shRNA lentiviral particles to the culture for 48 hours as per the manufacturer's instructions. Stable clones expressing the specific shRNAs were selected using 5μg/ml of puromycin (Gibco-life technologies) and pooled to generate the cells used in the experiments.

Immunofluorescence—Cells were grown on coverslips, fixed in 4% paraformaldehyde for 20 min, permeabilized with 0.2% Triton X100 for 10 mins, washed 3 times with PBS and incubated with primary antibody overnight at 4°C. The cells were then washed 3 times with PBS and incubated with secondary antibody for 1 hour at room temperature. After washing, coverslips were mounted using Prolong Gold antifade reagent with DAPI (Invitrogen). Confocal microscopy images were obtained using a Zeiss 780 confocal microscope. 3D Super-resolution structured illumination microscopy (SIM) imaging were performed with

Zeiss LSM710 ElyraP1 using alpha Plan-Apochromat 63X/1.40 oil objective lens. Images were taken using 3 rotations of SIM grating period and rendered with Zen 2012 SP2 software. In Z-stack images, Insets on top and right side of each image represent z-stacks in 2 different orientations; apical side of cell facing down on top inset and to left in side inset. Primary antibodies included those against: MAL2 (bs-7175R) from Bioss (Woburn, MA); NHERF1 (sc-134485), HA probe (sc-7392), FLAG probe (sc-166355), FOXO1 (sc-11350)from Santa Cruz (Dallas, Texas); PMCA2 (PA1-915), HER2 (MA1-35720) from Thermo Scientific (Waltham, MA); Ezrin (3145S), phospho-Ezrin (Thr567) (3141S), phospho-HER2 (thr1221/1222) (2243S), EGFR (4267S), HA probe (3724S), AKT (4691S), phosphor-AKT (4060S) from Cell Signaling (Danvers, MA); We also stained for lipid rafts using Cholera toxin subunit B, alexa fluor 555 conjugate (1423066) from Invitrogen (Grand Island, NY) and for actin using phalloidin-Atto 665 (04497) from Sigma (Buchs SG Switzerland).

Immunoblotting—Protein samples were prepared from cells using standard methods, were subjected to SDS-PAGE and transferred to a nitrocellulose membrane by wet Wwestern blot transfer (Bio-Rad). The membrane was blocked in TBST buffer (TBS + 1% Tween) containing 5% milk for 1 hour at room temperature. The blocked membranes were incubated overnight at 4°C with specific primary antibodies (Odyssey blocking buffer, 927-40000). The membranes were washed 3 times with TBST buffer, and then incubated with specific secondary antibodies provided by LI-COR for 2 hours at room temperature. After 3 washes with TBST buffer, the membranes were analyzed using the ODYSSEY Infrared Imaging system (LI-COR). All immunoblot experiments were performed at least 3 times and representative blots are shown in the figures. Primary antibodies included those against: phospho-HER2 (thr1221/1222) (2243S), EGFR (4267S), AKT (4691S), phospho-AKT (4060S) from Cell Signaling (Danvers, MA); HER2 (sc-33684), phospho-EGFR (sc-12351), flotillin1 (sc-25506) from Santa Cruz (Dallas, Texas); PMCA2 (PA1-915) from Thermo Scientific (Waltham, MA).

Co-immunoprecipitation—Cells were lysed with RIPA buffer (1% NP-40, 0.5% sodium deoxycholate, 0.1% SDS, 20 mM Tris Hcl, and 150 mM NaCl). Cell extracts were subsequently incubated overnight at 4°C with protein A/G beads (sc-2003, Santa Cruz) and the specific antibody (HSP90 (379400) from Invitrogen (Grand Island, NY)). After centrifugation, the immunoprecipitated proteins were eluted with LDS sample buffer containing 10% beta-mercaptoethanol to reverse the crosslinking. The resulting samples were then analyzed by Western blot.

Immunoprecipitation and mass spectrometry measurement—The immunoprecipitation was performed with the HER2 antibody (sc-33684) from Santa Cruz (Dallas, Texas). The elution samples from IP containing HER2 and its potential interactors in different cells were loaded onto the SDS-PAGE gel. The gel lanes and bands were processed by following a standard gel-based digestion protocol and digested with sequencing grade porcine trypsin (Promega) at 10 ng/ul overnight at 37°C. The amount of the final peptides was determined by Nanodrop (Thermo Scientific). About 1 ug of the total peptide digest from each sample were used for DIA-MS measurement on an

Orbitrap Fusion Lumos Tribrid mass spectrometer (Thermo Scientific) platform coupled to a nanoelectrospray ion source, as described previously. DIA-MS data analyses were performed using Spectronaut v13, by searching against the human Uniprot database. The Oxidation at methionine was set as variable modification, whereas carbamidomethylation at cysteine was set as a fixed modification. Both peptide and protein FDR cutoff (Qvalue) were controlled at 1%, and the label-free protein quantification was performed using the default settings in Spectronaut.

Proximity ligation assays—Proximity ligation assays (PLA) were performed using the Duolink™ assay kit (Sigma). SkBR3 cells were seeded onto 22 mm round collagen-coated coverslips (Corning, Cat N 354089). The experiments were performed when the cells reached 80% confluence. The cells were washed 3 times with PBS and paraformaldehyde (4% in PBS) was added to each well for 20 min, after which they were permeabilized with 0.2% Triton X100 in PBS. Permeabilized cells were incubated with combinations of the following antibodies: HER2 (MA1-35720), MAL2 (bs-7175R), NHERF1 (sc-134485), PMCA2 (PA1-915), Ezrin (3145S) and EGFR (4267S). PLA probes were then added and the assay was performed as per the manufacturer's instructions. All images were obtained using a Zeiss 780 confocal microscope. Quantification was done by measuring the intensity of fluorescence at randomly chosen phalloidin positive area at the plasma membrane.

Single-cell RNA-Sequencing (scRNA-Seq) data analysis—scRNA-Seq data of primary breast cancers were acquired from the GEO database (Accession: GSE75688). Sequencing reads were aligned to the human reference genome hg19 with HISAT2 v2.1.0 and a raw count table was generated by StringTie v2.0. Seurat v3.1.0 was used for quality controls and low-quality cells with >50% mitochondrial gene counts, <200 unique feature counts and doublets were excluded from the downstream analysis. The data was log-normalized by the total expression and highly variable features were selected for Principal Component Analysis (PCA) analysis. Prior to PCA, a linear transformation was applied to the data and statistically significant PCs were selected as inputs for Uniform Manifold Approximation and Projection (UMAP) to visualize the datasets after dimensional reduction. Markers defining each cluster were identified by comparing cells in one cluster to the ones in all other cells using Wilcoxon test.

ATAC-seq analysis—ATAC-seq libraries from SKBR3 cells were constructed with 50 K cells following Omni-ATAC protocol (Illumina FC-121-1031). The libraries were sequenced on Illumina Nextseq 500 (paired-end run, 42 bp). Sequenced reads were trimmed with adaptor sequences (cutadapt v1.9.1) and mapped to the human genome (GRCh38, ensembl release 99) by Bowtie2 (v2.3.4.1). Mitochondrial and duplicated reads were removed by SAMtools (v1.9) and Picard (v2.9.0, https://broadinstitute.github.io/picard/) tools, respectively. Peaks were found by MACS2 (v.2.1.1) and visualized by deepTools (v3.1.1).

Raw ATAC-Seq data for MCF10A (Accession: GSE89013), MCF-7 (Accession: GSE117940), and MDA-MB-231 (Accession: GSE129646) were downloaded from the GEO database. Sequencing reads were trimmed for adapters using trimmomatic and aligned to the human reference genome hg19 using Bowtie2 with default parameters. PCR duplicates

were marked with Picard tools. Peaks were called using MACS2 (v.2.1.1) and split at the summits using an in-house R script. For differential accessibility analysis, reads that were mapped at each consensus peak were counted for each biological replicate and analyzed with DESeq2. P-values were corrected for multiple testing by the Benjamini-Hochberg procedure and Peaks with the adjusted p -value < 0.05 were considered as significantly differential. BigWig files from each dataset were loaded onto the Integrated Genomics Viewer (IGV) and ATAC-Seq peaks were visualized.

Microarray analysis—Raw microarray data were downloaded from the GEO database (GES62555). Differentially expressed genes (DEGs) were identified with limma. A volcano plot was generated using the EnhancedVolcano R package. The expression of MAL2 and FLOT1 was visualized by the pheatmap R package (R Kolde-R package version, 2012).

QUANTIFICATION AND STATISTICAL ANALYSIS

The number of repeats (n) refers to the number of independent experimental observations in each figure legend. Statistical analyses were performed with Prism 6.0 (GraphPad Software, La Jolla, CA). Except for scRNA-Seq and ATAC-Seq analyses (see above), statistical significance was determined using unpaired t test for comparisons between 2 groups and one-way ANOVA for groups of 3 or more. Group data were presented as mean±SEM. The p values less than 0.05 (indicated by *), or less than 0.01 (**), or less than 0.001 (***), or less than 0.0001 (****) were considered as significant.

Supplementary Material

Refer to Web version on PubMed Central for supplementary material.

ACKNOWLEDGMENTS

REFERENCES

Akerboom J, Chen TW, Wardill TJ, Tian L, Marvin JS, Mutlu S, Calderon NC, Esposti F, Borghuis BG, Sun XR, et al. (2012). Optimization of a GCaMP calcium indicator for neural activity imaging. J. Neurosci 32, 13819–13840. 10.1523/JNEUROSCI.2601-12.2012. [PubMed: 23035093]

Alawin OA, Ahmed RA, Ibrahim BA, Briski KP, and Sylvester PW (2016). Antiproliferative effects of gamma-tocotrienol are associated with lipid raft disruption in HER2-positive human breast cancer cells. J. Nutr. Biochem 27, 266–277. 10.1016/j.jnutbio.2015.09.018. [PubMed: 26507543]

Alonso MA, and Millan J (2001). The role of lipid rafts in signalling and membrane trafficking in T lymphocytes. J. Cell Sci 114, 3957–3965. [PubMed: 11739628]

Arteaga CL, and Engelman JA (2014). ERBB receptors: from oncogene discovery to basic science to mechanism-based cancer therapeutics. Cancer Cell 25, 282–303. 10.1016/j.ccr.2014.02.025. [PubMed: 24651011]

Arteaga CL, Sliwkowski MX, Osborne CK, Perez EA, Puglisi F, and Gianni L (2011). Treatment of HER2-positive breast cancer: current status and future perspectives. Nat. Rev. Clin. Oncol 9, 16–32. 10.1038/nrclinonc.2011.177. [PubMed: 22124364]

Asp N, Pust S, and Sandvig K (2014). Flotillin depletion affects ErbB protein levels in different human breast cancer cells. Biochim. Biophys. Acta 1843, 1987–1996. 10.1016/j.bbamcr.2014.04.013. [PubMed: 24747692]

Barok M, Joensuu H, and Isola J (2014). Trastuzumab emtansine: mechanisms of action and drug resistance. Breast Cancer Res. 16, 209. 10.1186/bcr3621. [PubMed: 24887180]

Bertelsen V, and Stang E (2014). The mysterious ways of ErbB2/HER2 trafficking. Membranes (Basel) 4, 424–446. 10.3390/membranes4030424. [PubMed: 25102001]

Bhandari A, Shen Y, Sindan N, Xia E, Gautam B, Lv S, and Zhang X (2018). MAL2 promotes proliferation, migration, and invasion through regulating epithelial-mesenchymal transition in breast cancer cell lines. Biochem. Biophys. Res. Commun 504, 434–39. 10.1016/j.bbrc.2018.08.187. [PubMed: 30195491]

Bosk S, Braunger JA, Gerke V, and Steinem C (2011). Activation of F-actin binding capacity of Ezrin: synergism of PIP(2) interaction and phosphorylation. Biophys. J 100, 1708–1717. 10.1016/j.bpj.2011.02.039. [PubMed: 21463584]

Brown DA (2006). Lipid rafts, detergent-resistant membranes, and raft targeting signals. Physiology (Bethesda) 21, 430–439. 10.1152/physiol.00032.2006. [PubMed: 17119156]

Butler A, Hoffman P, Smibert P, Papalexi E, and Satija R (2018). Integrating single-cell transcriptomic data across different conditions, technologies, and species. Nat. Biotechnol 36, 411–420. [PubMed: 29608179]

Cai WL, Greer CB, Chen JF, Arnal-Estapé A, Cao J, Yan Q, and Nguyen DX (2020). Specific chromatin landscapes and transcription factors couple breast cancer subtype with metastatic relapse to lung or brain. BMC Med. Genomics 13, 33. [PubMed: 32143622]

Chung W, Eum HH, Lee HO, Lee KM, Lee HB, Kim KT, Ryu HS, Kim S, Lee JE, Park YH, et al. (2017). Single-cell RNA-seq enables comprehensive tumour and immune cell profiling in primary breast cancer. Nat. Commun 8, 15081. 10.1038/ncomms15081. [PubMed: 28474673]

Cuello M, Ettenberg SA, Clark AS, Keane MM, Posner RH, Nau MM, Dennis PA, and Lipkowitz S (2001). Down-regulation of the erbB-2 receptor by trastuzumab (herceptin) enhances tumor necrosis factor-related apoptosis-inducing ligand-mediated apoptosis in breast and ovarian cancer cell lines that overexpress erbB-2. Cancer Res. 61, 4892–900. [PubMed: 11406568]

de Marco MC, Martin-Belmonte F, Kremer L, Albar JP, Correas I, Vaerman JP, Marazuela M, Byrne JA, and Alonso MA (2002). MAL2, a novel raft protein of the MAL family, is an essential component of the machinery for transcytosis in hepatoma HepG2 cells. J. Cell Biol 159, 37–44. 10.1083/jcb.200206033. [PubMed: 12370246]

de Melo Gagliato D, Jardim DL, Marchesi MS, and Hortobagyi GN (2016). Mechanisms of resistance and sensitivity to anti-HER2 therapies in HER2+ breast cancer. Oncotarget 7, 64431–64446. 10.18632/oncotarget.7043. [PubMed: 26824988]

Derakhshani A, Rezaei Z, Safarpour H, Sabri M, Mir A, Sanati MA, Vahidian F, Gholamiyan Moghadam A, Aghadoukht A, Hajiasgharzadeh K, and Baradaran B (2020). Overcoming trastuzumab resistance in HER2-positive breast cancer using combination therapy. J. Cell Physiol 235, 3142–3156. 10.1002/jcp.29216. [PubMed: 31566722]

Elliott BE, Meens JA, SenGupta SK, Louvard D, and Arpin M (2005). The membrane cytoskeletal crosslinker Ezrin is required for metastasis of breast carcinoma cells. Breast Cancer Res. 7, R365–R373. 10.1186/bcr1006. [PubMed: 15987432]

Escriva-de-Romani S, Arumi M, Bellet M, and Saura C (2018). HER2-positive breast cancer: current and new therapeutic strategies. Breast 39, 80–88. 10.1016/j.breast.2018.03.006. [PubMed: 29631097]

Gale M, Li Y, Cao J, Liu ZZ, Holmbeck MA, Zhang M, Lang SM, Wu L, Do Carmo M, Gupta S, et al. (2020). Acquired resistance to HER2-targeted therapies creates vulnerability to ATP synthase inhibition. Cancer Res. 80, 524–535. 10.1158/0008-5472.CAN-18-3985. [PubMed: 31690671]

Gomes L, Sorgine M, Passos CLA, Ferreira C, de Andrade IR, Silva JL, Atella GC, Mermelstein CS, and Fialho E (2019). Increase in fatty acids and flotillins upon resveratrol treatment of human breast cancer cells. Sci. Rep 9, 13960. 10.1038/s41598-019-50416-5. [PubMed: 31562347]

Guan J, Zhou W, Hafner M, Blake RA, Chalouni C, Chen IP, De Bruyn T, Giltnane JM, Hartman SJ, Heidersbach A, et al. (2019). Therapeutic Ligands Antagonize Estrogen Receptor Function by Impairing Its Mobility. Cell 178, 949–963.e18. [PubMed: 31353221]

Guy CT, Webster MA, Schaller M, Parsons TJ, Cardiff RD, and Muller WJ (1992). Expression of the neu protooncogene in the mammary epithelium of transgenic mice induces metastatic disease. Proc. Natl. Acad. Sci. U S A 89, 10578–10582. [PubMed: 1359541]

Hanker AB, Cook RS, and Arteaga CL (2013). Mouse models and anti-HER2 therapies. Oncotarget 4, 1866–1867. 10.18632/oncotarget.1481. [PubMed: 24272818]

Heinz S, Benner C, Spann N, Bertolino E, Lin YC, Laslo P, Cheng JX, Murre C, Singh H, and Glass CK (2010). Simple combinations of lineage-determining transcription factors prime cis-regulatory elements required for macrophage and B cell identities. Mol. Cell 38, 576–589. [PubMed: 20513432]

Hemler ME (2003). Tetraspanin proteins mediate cellular penetration, invasion, and fusion events and define a novel type of membrane microdomain. Annu. Rev. Cell Dev Biol 19, 397–22. 10.1146/annurev.cell-bio.19.111301.153609. [PubMed: 14570575]

Hynes NE, and MacDonald G (2009). ErbB receptors and signaling pathways in cancer. Curr. Opin. Cell Biol 21, 177–184. 10.1016/j.ceb.2008.12.010. [PubMed: 19208461]

Janke M, Herrig A, Austermann J, Gerke V, Steinem C, and Janshoff A (2008). Actin binding of Ezrin is activated by specific recognition of PIP2-functionalized lipid bilayers. Biochemistry 47, 3762–3769. 10.1021/bi702542s. [PubMed: 18302339]

Jayasundar JJ, Ju JH, He L, Liu D, Meilleur F, Zhao J, Callaway DJ, and Bu Z (2012). Open conformation of Ezrin bound to phosphatidylinositol 4,5-bisphosphate and to F-actin revealed by neutron scattering. J. Biol. Chem 287, 37119–37133. 10.1074/jbc.M112.380972. [PubMed: 22927432]

Jeong J, Choi J, Kim W, Dann P, Takyar F, Gefter JV, Friedman PA, and Wysolmerski J (2018). Inhibition of Ezrin causes PKCalpha-mediated internalization of erbb2/HER2 tyrosine kinase in breast cancer cells. J. Biol. Chem 294, 887–901. 10.1074/jbc.RA118.004143. [PubMed: 30463939]

Jeong J, Kim W, Kim LK, VanHouten J, and Wysolmerski JJ (2017a). HER2 signaling regulates HER2 localization and membrane retention. PLoS One 12, e0174849. 10.1371/journal.pone.0174849. [PubMed: 28369073]

Jeong J, VanHouten JN, Dann P, Kim W, Sullivan C, Yu H, Liotta L, Espina V, Stern DF, Friedman PA, and Wysolmerski JJ (2016). PMCA2 regulates HER2 protein kinase localization and signaling and promotes HER2-mediated breast cancer. Proc. Natl. Acad. Sci. U S A 113, E282–E290. 10.1073/pnas.1516138113. [PubMed: 26729871]

Jeong J, VanHouten JN, Kim W, Dann P, Sullivan C, Choi J, Sneddon WB, Friedman PA, and Wysolmerski JJ (2017b). The scaffolding protein NHERF1 regulates the stability and activity of the tyrosine kinase HER2. J. Biol. Chem 292, 6555–6568. 10.1074/jbc.M116.770883. [PubMed: 28235801]

Klapper LN, Waterman H, Sela M, and Yarden Y (2000). Tumor-inhibitory antibodies to HER-2/ErbB-2 may act by recruiting c-Cbl and enhancing ubiquitination of HER-2. Cancer Res. 60, 3384–3388. [PubMed: 10910043]

Koninki K, Barok M, Tanner M, Staff S, Pitkanen J, Hemmila P, Ilvesaro J, and Isola J (2010). Multiple molecular mechanisms underlying trastuzumab and lapatinib resistance in JIMT-1 breast cancer cells. Cancer Lett. 294, 211–219. 10.1016/j.canlet.2010.02.002. [PubMed: 20193978]

Lajoie P, and Nabi IR (2010). Lipid rafts, caveolae, and their endocytosis. Int. Rev. Cell Mol Biol 282, 135–163. 10.1016/S1937-6448(10)82003-9.

Li BT, Michelini F, Misale S, Cocco E, Baldino L, Cai Y, Shifman S, Tu HY, Myers ML, Xu C, et al. (2020). HER2-Mediated internalization of cytotoxic agents in ERBB2 amplified or mutant lung cancers. Cancer Discov. 10, 674–687. 10.1158/2159-8290.CD-20-0215. [PubMed: 32213539]

Langmead B, and Salzberg S (2012). Fast gapped-read alignment with Bowtie 2. Nat. Methods 4, 357–359.

Li H, Handsaker B, Wysoker A, Fennell T, Ruan J, Homer N, Marth G, Abecasis G, and Durbin R; 1000 Genome Project Data Processing Subgroup (2009). The Sequence Alignment/Map format and SAMtools. Bioinformatics 25, 2078–2079. [PubMed: 19505943]

Li J, Li Y, Liu H, Liu Y, and Cui B (2017). The four-transmembrane protein MAL2 and tumor protein D52 (TPD52) are highly expressed in colorectal cancer and correlated with poor prognosis. PLoS One 12, e0178515. 10.1371/journal.pone.0178515. [PubMed: 28562687]

Li YC, Park MJ, Ye SK, Kim CW, and Kim YN (2006). Elevated levels of cholesterol-rich lipid rafts in cancer cells are correlated with apoptosis sensitivity induced by cholesterol-depleting agents. Am. J. Pathol 168, 1107–1118, quiz 1404-1105. 10.2353/ajpath.2006.050959. [PubMed: 16565487]

Lin C, Wu Z, Lin X, Yu C, Shi T, Zeng Y, Wang X, Li J, and Song L (2011). Knockdown of FLOT1 impairs cell proliferation and tumorigenicity in breast cancer through upregulation of FOXO3a. Clin. Cancer Res. 17, 3089–3099. 10.1158/1078-0432.CCR-10-3068. [PubMed: 21447726]

Liu Y, Walavalkar NM, Dozmorov MG, Rich SS, Civelek M, and Guertin MJ (2017). Identification of breast cancer associated variants that modulate transcription factor binding. Plos Genet 13, e1006761. [PubMed: 28957321]

Magal LG, Yaffe Y, Shepshelovich J, Aranda JF, de Marco Mdel C, Gaus K, Alonso MA, and Hirschberg K (2009). Clustering and lateral concentration of raft lipids by the MAL protein. Mol. Biol. Cell 20, 3751–3762. 10.1091/mbc.E09-02-0142. [PubMed: 19553470]

Marazuela M, and Alonso MA (2004). Expression of MAL and MAL2, two elements of the protein machinery for raft-mediated transport, in normal and neoplastic human tissue. Histol. Histopathol 19, 925–933. 10.14670/HH-19.925. [PubMed: 15168355]

Martin M (2011). Cutadapt removes adapter sequences from high-throughput sequencing reads. EMBnet.journal. 10.14806/ej.17.1.200.

Mollinedo F, and Gajate C (2015). Lipid rafts as major platforms for signaling regulation in cancer. Adv. Biol. Regul 57, 130–146. 10.1016/j.jbior.2014.10.003. [PubMed: 25465296]

Mollinedo F, and Gajate C (2020). Lipid rafts as signaling hubs in cancer cell survival/death and invasion: implications in tumor progression and therapy. J. Lipid Res 61, 611–635. 10.1194/jlr.TR119000439. [PubMed: 33715811]

Nagy P, Vereb G, Sebestyen Z, Horvath G, Lockett SJ, Damjanovich S, Park JW, Jovin TM, and Szollosi J (2002). Lipid rafts and the local density of ErbB proteins influence the biological role of homo-and heteroassociations of ErbB2. J. Cell Sci 115, 4251–262. 10.1242/jcs.00118. [PubMed: 12376557]

Olayioye MA (2001). Update on HER-2 as a target for cancer therapy: intracellular signaling pathways of ErbB2/HER-2 and family members. Breast Cancer Res. 3, 385–389. 10.1186/bcr327. [PubMed: 11737890]

Ou YX, Liu FT, Chen FY, and Zhu ZM (2017). Prognostic value of Flotillin-1 expression in patients with solid tumors. Oncotarget 8, 52665–52677. 10.18632/oncotarget.17075. [PubMed: 28881760]

Patel HH, and Insel PA (2009). Lipid rafts and caveolae and their role in compartmentation of redox signaling. Antioxid. Redox Signal. 11, 1357–1372. 10.1089/ARS.2008.2365. [PubMed: 19061440]

Pereira PMR, Sharma SK, Carter LM, Edwards KJ, Pourat J, Ragupathi A, Janjigian YY, Durack JC, and Lewis JS (2018). Caveolin-1 mediates cellular distribution of HER2 and affects trastuzumab binding and therapeutic efficacy. Nat. Commun. 9, 5137. 10.1038/s41467-018-07608-w. [PubMed: 30510281]

Pertea M, Pertea GM, Antonescu CM, Chang T-C, Mendell JT, and Salzberg SL (2015). StringTie enables improved reconstruction of a transcriptome from RNA-seq reads. Nat. Biotechnol. 33, 290–295. [PubMed: 25690850]

Pike LJ (2003). Lipid rafts: bringing orderto chaos. J. Lipid Res. 44, 655–667. 10.1194/jlr.R200021-JLR200. [PubMed: 12562849]

Pike LJ (2005). Growth factor receptors, lipid rafts and caveolae: an evolving story. Biochim. Biophys. Acta 1746, 260–273. 10.1016/j.bbamcr.2005.05.005. [PubMed: 15951036]

Pust S, Klokk TI, Musa N, Jenstad M, Risberg B, Erikstein B, Tcatchoff L, Liestol K, Danielsen HE, van Deurs B, and Sandvig K (2013). Flotillins as regulators of ErbB2 levels in breast cancer. Oncogene 32, 3443–3451. 10.1038/onc.2012.357. [PubMed: 22869152]

Quan C, Sun J, Lin Z, Jin T, Dong B, Meng Z, and Piao J (2019). Ezrin promotes pancreatic cancer cell proliferation and invasion through activating the Akt/mTOR pathway and inducing YAP translocation. Cancer Manag. Res 11, 6553–6566. 10.2147/CMAR.S202342. [PubMed: 31372056]

Ramírez F, Ryan DP, Grüning B, Bhardwaj V, Kilpert F, Richter AS, Heyne S, Dündar F, and Manke T (2016). deepTools2: a next generation web server for deep-sequencing data analysis. Nucleic Acids Res 44, W160–W165. [PubMed: 27079975]

Robinson JT, Thorvaldsdóttir H, Winckler W, Guttman M, Lander ES, Getz G, Mesirovet, et al. (2011). Integrative Genomics Viewer. Nat. Biotechnol 29, 24–26. [PubMed: 21221095]

Schuck S, Honsho M, Ekroos K, Shevchenko A, and Simons K (2003). Resistance of cell membranes to different detergents. Proc. Natl. Acad. Sci. U S A 100, 5795–5800. 10.1073/pnas.0631579100. [PubMed: 12721375]

Schuck S, and Simons K (2004). Polarized sorting in epithelial cells: raft clustering and the biogenesis of the apical membrane. J. Cell Sci 117, 5955–5964. 10.1242/jcs.01596. [PubMed: 15564373]

Shehata M, Bieche I, Boutros R, Weidenhofer J, Fanayan S, Spalding L, Zeps N, Byth K, Bright RK, Lidereau R, and Byrne JA (2008). Nonredundant functions for tumor protein D52-like proteins support specific targeting of TPD52. Clin. Cancer Res 14, 5050–5060. 10.1158/1078-0432.CCR-07-4994. [PubMed: 18698023]

Shigetomi E, Kracun S, and Khakh BS (2010). Monitoring astrocyte calcium microdomains with improved membrane targeted GCaMP reporters. Neuron Glia Biol. 6, 183–191. 10.1017/S1740925X10000219. [PubMed: 21205365]

Simons K, and Sampaio JL (2011). Membrane organization and lipid rafts. Cold Spring Harb. Perspect. Biol 3, a004697. 10.1101/cshperspect.a004697. [PubMed: 21628426]

Staubach S, and Hanisch FG (2011). Lipid rafts: signaling and sorting platforms of cells and their roles in cancer. Expert Rev. Proteomics 8, 263–277. 10.1586/epr.11.2. [PubMed: 21501018]

Tanner M, Kapanen AI, Junttila T, Raheem O, Grenman S, Elo J, Elenius K, and Isola J (2004). Characterization of a novel cell line established from a patient with herceptin-resistant breast cancer. Mol. Cancer Ther 3, 1585–1592. [PubMed: 15634652]

Vernieri C, Milano M, Brambilla M, Mennitto A, Maggi C, Cona MS, Prisciandaro M, Fabbroni C, Celio L, Mariani G, et al. (2019). Resistance mechanisms to anti-HER2 therapies in HER2-positive breast cancer: current knowledge, new research directions and therapeutic perspectives. Crit. Rev. Oncol. Hematol 139, 53–66. 10.1016/j.critrevonc.2019.05.001. [PubMed: 31112882]

Highlights

- MAL2 is required for HER2 membrane retention and signaling in breast cancer cells

- MAL2 strengthens the formation of the HER2/Ezrin/NHERF1/PMCA2 protein complex

- Loss of MAL2 increases plasma membrane calcium concentration

- HER2/MAL2 interaction is enhanced in trastuzumab-resistant breast cancer cells
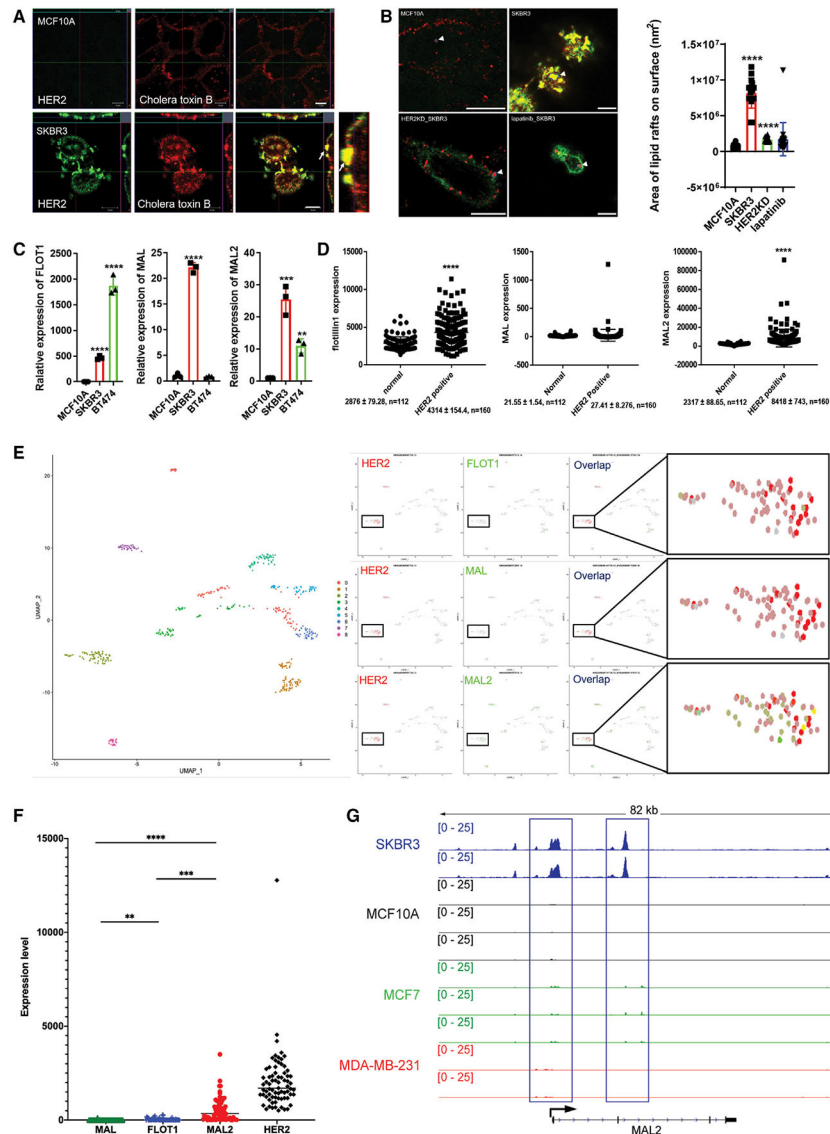
Figure 1. Associations between HER2 and MAL2 in lipid raft-rich membrane protrusions

(A) Immunofluorescence staining for HER2 and cholera toxin B in MCF10A and SKBR3 cells. Scale bars represent 10 μm.

(B) Lipid raft areas on the cell surface, with quantification in the bar graph on the right.

(C) Flotillin1 (FLOT1), MAL, and MAL2 mRNA expression in different breast cancer cell lines as assessed by quantitative PCR (n = 3).

(D) RNA-seq analysis of FLOT1 and MAL2 expression in normal breast tissue (n = 112) and HER2-positive breast tumors (n = 160) represented in The Cancer Genome Atlas database.

(E) Uniform Manifold Approximation and Projection (UMAP) plots of breast cancer single-cell RNA-seq data (GEO: GSE75688, left) and co-expression pattern of HER2, FLOT1, MAL, and MAL2 in cells from cluster 2.

(F) Distribution of MAL, FLOT1, MAL2, and HER2 expression level for each cell in cluster 2.

(G) MAL2 ATAC-seq peak clusters in SKBR3, MCF10A, MCF7, and MDA-MB-231 cell lines. In the bar graphs, the bars represent the mean ± SEM. **p <0.01, ***p <0.001, ****p <0.0001. These results are representative of three independent experiments.
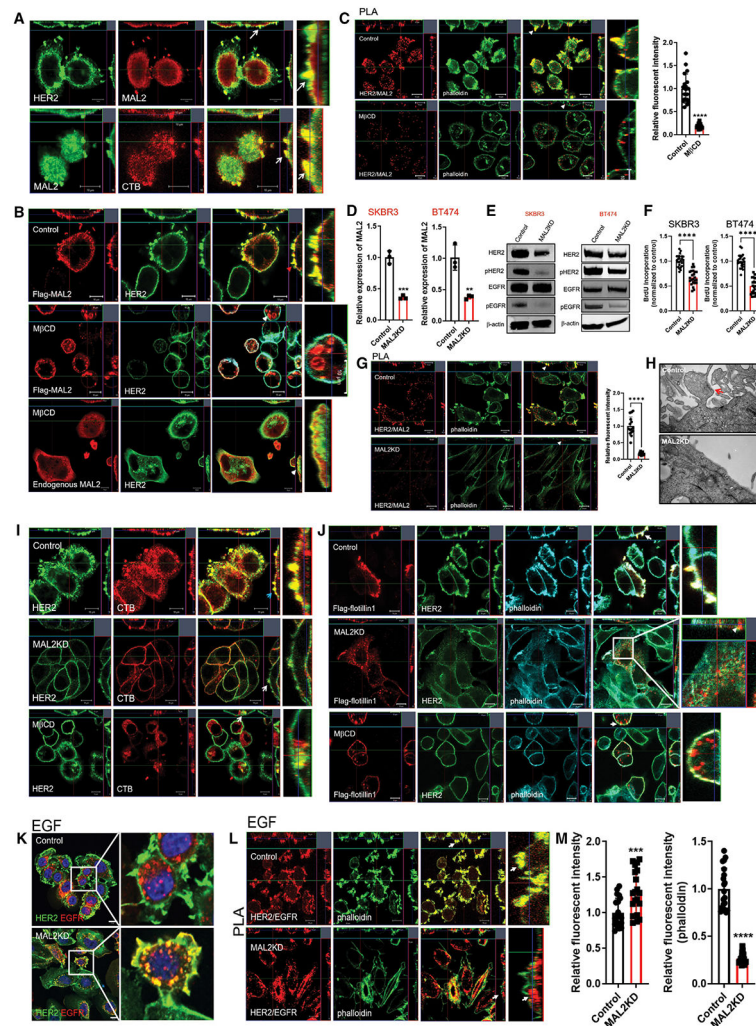
Figure 2. MAL2 expression is required for formation of lipid raft-enriched membrane protrusions

(A) Immunofluorescence staining for HER2 and MAL2 (top row) and MAL2 and cholera toxin B (lipid rafts) (bottom row) in SKBR3 cells.

(B) Immunofluorescence staining for FLAG-tagged MAL2 or endogenous MAL2 with HER2 and actin in control and MβCD (5 mM)-treated SKBR3 cells. Scale bars represent 10 μm.

(C) Proximity ligation assay (PLA) experiment for HER2 and MAL2 in control and MβCD (5 mM)-treated SKBR3 cells also stained for actin (phalloidin). Scale bars represent 10 μm.

(D) MAL2 mRNA expression in control and MAL2 knockdown SKBR3 and BT474 cells as assessed by quantitative RT-PCR (n = 3).

(E) Western blot analysis of HER2, phospho-HER2, EGFR, and phospho-EGFR in control and MAL2 knockdown SKBR3 and BT474 cells.

(F) BrdU incorporation in MAL2KD cells relative to control SKBR3 and BT474 cells.

(G) PLA experiment for HER2 and MAL2 in control and MAL2LD SKBR3 cells. Scale bars represent 10 μm.

(H) Transmission electron microscopy images in control and MAL2 knockdown SKBR3 cells.

(I) Immunofluorescence staining HER2 and cholera toxin B in control (top), MAL2KD-treated (middle), and MβCD-treated (5 mM) SKBR3 cells. Scale bars represent 10 μm.

(J) Immunofluorescence staining for FLAG-tagged FLOT1, HER2, and phalloidin in control, MAL2KD-treated, and MβCD (5 mM)-treated SKBR3 cells. Scale bars represent 10 μm.

(K) Immunofluorescence staining for HER2 and EGFR in control and MAL2KD SKBR3 cells. Scale bars represent 10 μm.

(L) PLA experiment for HER2 and EGFR in control and MAL2KD SKBR3 cells also stained for actin (phalloidin). Scale bars represent 10μm.

(M) Quantitation of PLA experiment by measuring fluorescent intensity of amplified PLA reactions and phalloidin. Bar graphs represent the mean ± SEM. **$p < 0.01$, ***$p < 0.001$, ****$p < 0.0001$. These results are representative of three independent experiments.
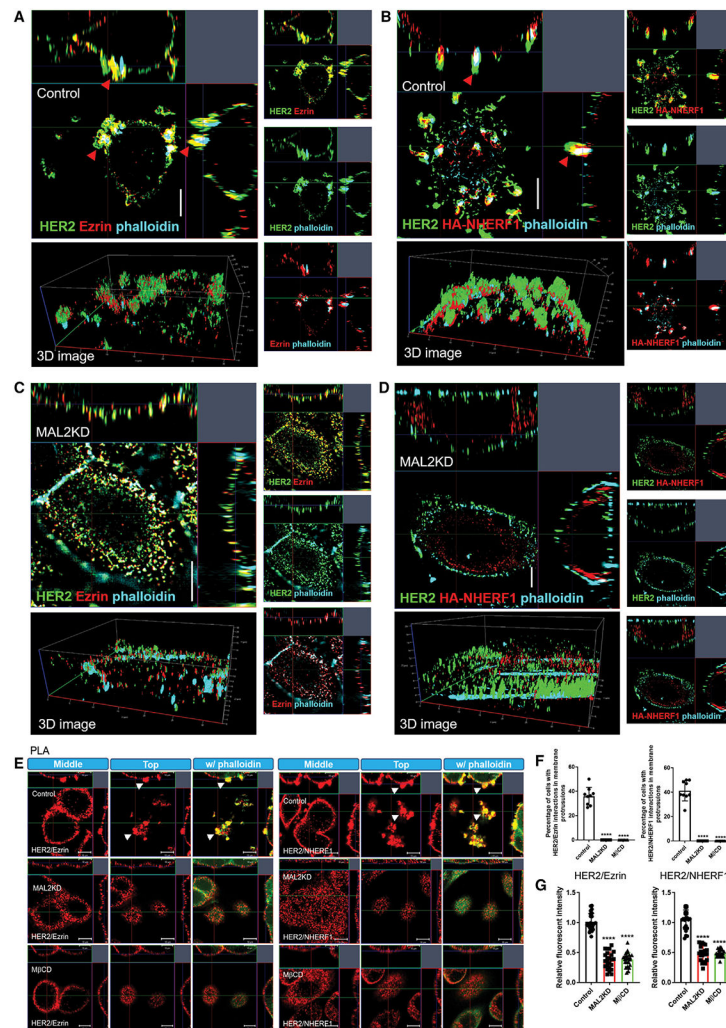
Figure 3. Organization of HER2/Ezrin/NHERF1/actin complexes requires MAL2 and lipid rafts

(A) SIM imaging of fluorescent staining for HER2, Ezrin, and phalloidin in control SKBR3 cells. Images represent different combinations of staining as noted on the figures. Bottom left: a 3D reconstruction for all three molecules. Scale bars represent 10 μm.

(B) SIM imaging of fluorescent staining for HER2, HA-tagged NHERF1, and phalloidin in control SKBR3 cells. Bottom left: a 3D reconstruction for all three molecules. Scale bars represent 10 μm.

(C) SIM imaging of fluorescent staining for HER2, Ezrin, and phalloidin in MAL2 knockdown SKBR3 cells. Scale bars represent 10 μm.

(D) SIM imaging of fluorescent staining for HER2, HA-tagged NHERF1, and phalloidin in MAL2 knockdown SKBR3 cells. Scale bars represent 10 μm.

(E) PLA for HER2 with Ezrin (left panels) or NHERF1 (right panels) in control (top row), MAL2 knockdown-treated (middle row) and MβCD-treated (bottom row) SKBR3 cells. Columns labeled "Middle" represent an optical section through the mid-portion of the cells. Columns labeled "Top" represent an optical section taken near the apical surface of the cell. Columns labeled "w/Phalloidin" represent co-registration of the PLA signal and immunofluorescence for actin (phalloidin). Scale bars represent 10 μm (for all images).

(F) Percentage of cells with positive PLA reactions located within membrane protrusions. (G) Quantitation of PLA fluorescent intensity within membrane protrusions. Bar graphs represent the mean ± SEM. ****p <0.0001. These results are representative of three independent experiments.
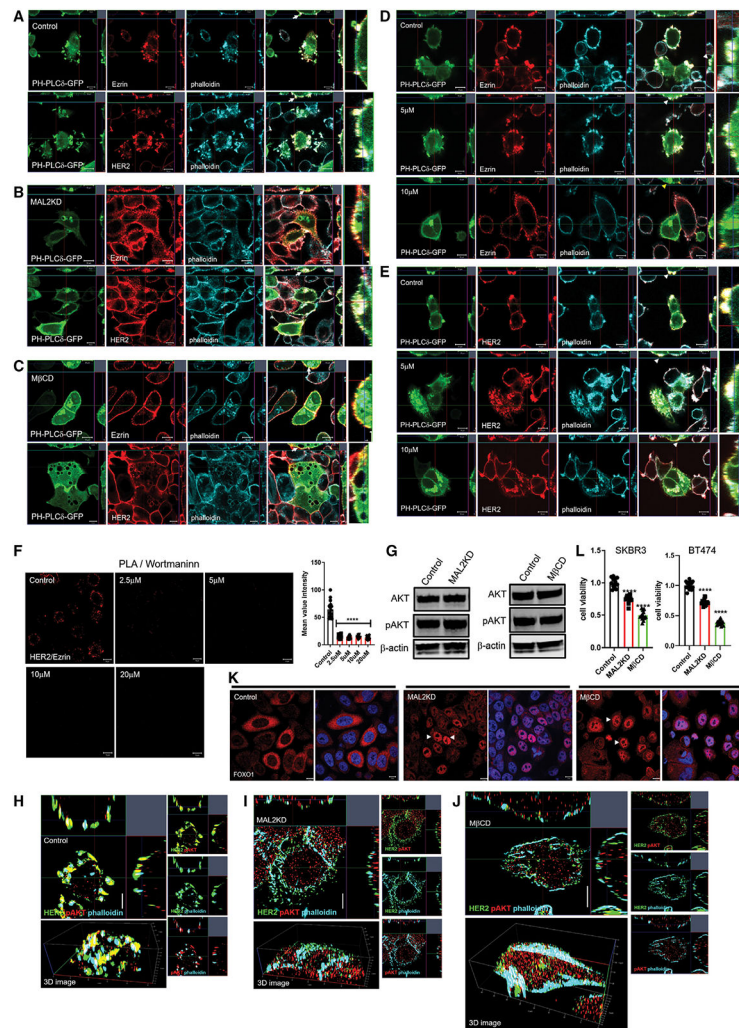
Figure 4. Enrichment of PIP2 and pAKT together with HER2 in membrane protrusions requires MAL2 and lipid rafts

(A) Co-immunofluorescence staining for Ezrin (top) or HER2 (bottom) with phalloidin in PH-PLCδ-GFP-expressing control SKBR3 cells. Scale bars represent 10 μm.

(B) Immunofluorescence staining for Ezrin (top) or HER2 (bottom) with phalloidin in PH-PLCδ-GFP-expressing MAL2KD_SKBR3 cells.

(C) Immunofluorescence staining for Ezrin (top) or HER2 (bottom) with phalloidin in PH-PLCδ-GFP-expressing SKBR3 cells treated with MβCD.

(D) Immunofluorescence staining for Ezrin with phalloidin in PH-PLCδ-GFP-expressing SKBR3 cells treated with wortmannin (0, 5, and 10 μM).

(E) Immunofluorescence staining for HER2 with phalloidin in PH-PLCδ-GFP-expressing SKBR3 cells treated with wortmannin (0, 5, and 10 μM).

(F) PLA results for HER2 and Ezrin in control and wortmannin-treated SKBR3 cells. Scale bars represent 10 μm.

(G) Western blot analysis of AKT and phospho-AKT in control and MAL2 knockdown SKBR3 cells (left) and in control and MβCD-treated SKBR3 cells (right).

(H–J) SIM imaging showing HER2, pAKT, and phalloidin immunofluorescence in control (H), MAL2KD (I)-treated, and MβCD-treated (J) SKBR3 cells. Scale bars represent 10 μm.

(K) Immunofluorescence staining for FOXO1 in control, MAL2KD-treated, and MβCD-treated SKBR3 cells.

(L) XTT cell viability assay in control, MAL2KD-treated, and MβCD-treated SKBR3 and BT474 cells. Bar graphs represent the mean ± SEM. ****$p < 0.0001$. These results are representative of three independent experiments.
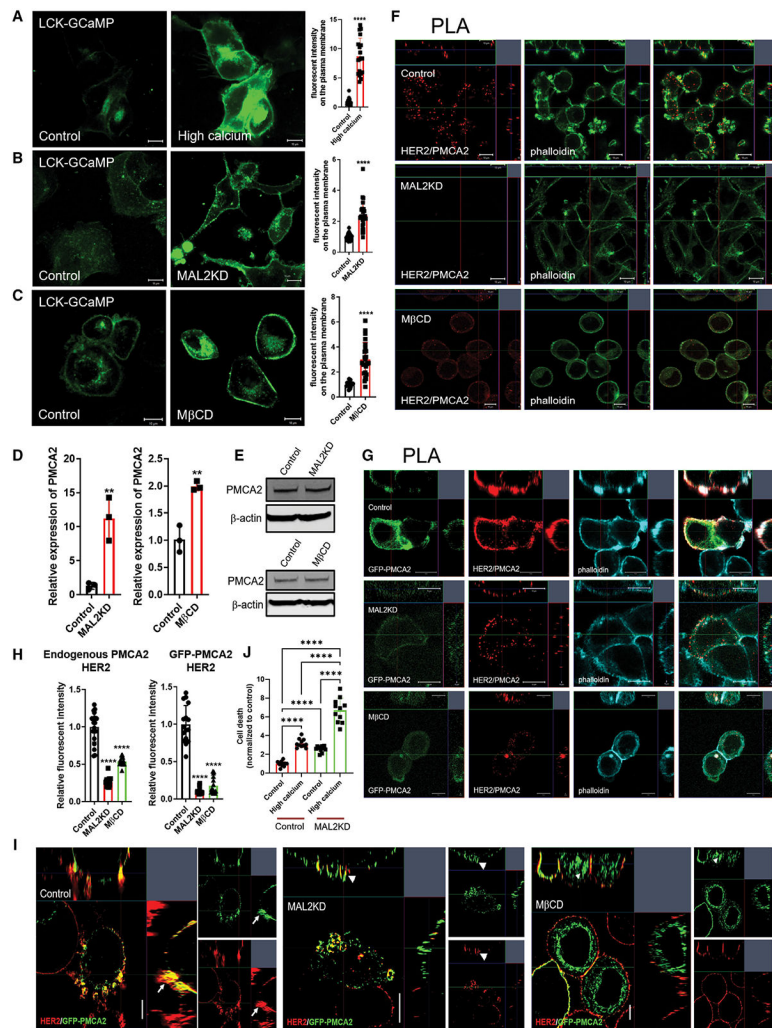
Figure 5. MAL2 and lipid rafts maintain interactions between HER2 and PMCA2 required to maintain low calcium concentrations at the plasma membrane

(A) Live cell confocal images in SKBR3 cells expressing LCK-GCaMP at physiologic calcium (control) or treated with 10 mM extracellular calcium + 10 μM ionomycin.

(B) Live cell confocal images in control and MAL2KD_SKBR3 cells expressing LCK-GCaMP.

(C) Live cell confocal images in control and MβCD-treated SKBR3 cells expressing LCK-GCaM.

(D) PMCA2 mRNA expression in control, MAL2KD-treated, or MβCD-treated SKBR3 cells as assessed by quantitative RT-PCR (n = 3).

(E) Western blot analysis of PMCA2 protein levels in control, MAL2KD-treated, or MβCD-treated SKBR3 cells.

(F) PLA with immunofluorescence for phalloidin in HER2 and PMCA2 in control (top row), MAL2KD-treated (middle row), and MβCD-treated (bottom row) SKBR3 cells. Scale bars represent 10 μm.

(G) PLA for HER2 and GFP-PMCA2 with immunofluorescence for GFP-labeled PMCA2 and actin (phalloidin) in control (top row), MAL2KD-treated (middle row), and MβCD-treated (bottom row) SKBR3 cells.

(H) Quantitation of PLA experiment from (F) and (G) by measuring the fluorescent intensity of amplified PLA reactions at the plasma membrane.

(I) SIM imaging showing HER2- and GFP-labeled PMCA2 in control, MAL2KD-treated, and MβCD-treated SKBR3 cells. Scale bars represent 10 μm.

(J) Apoptosis, as assessed by TUNEL assay, in MAL2KD cells relative to controls exposed to 5 mM calcium ± ionomycin. These results are the representative of three independent experiments.
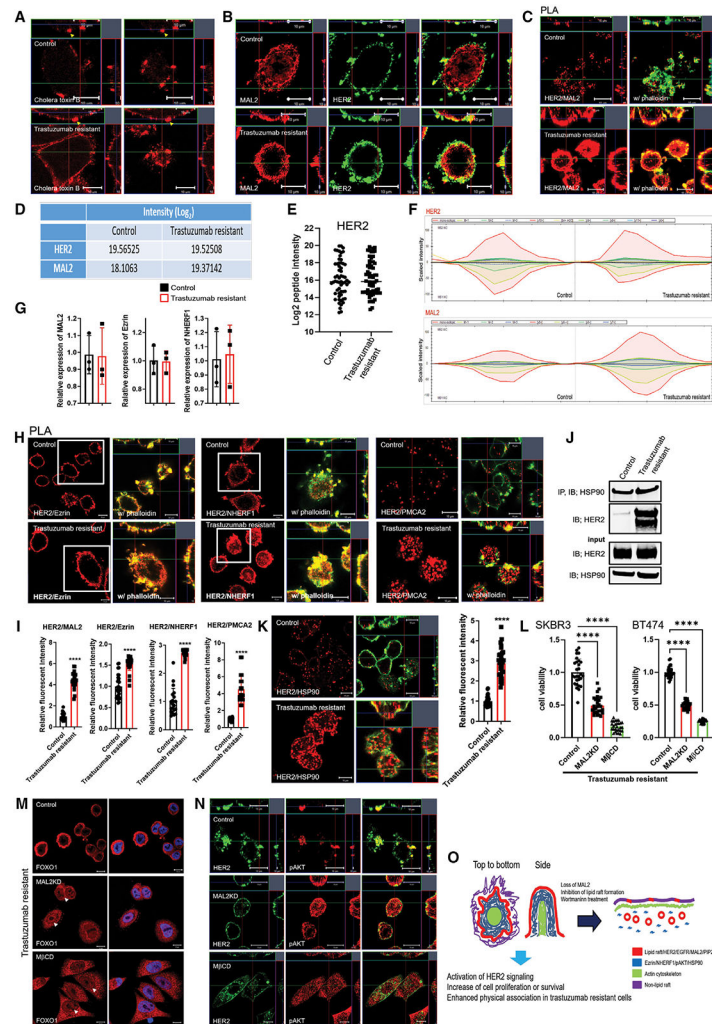
Figure 6. Enhanced interactions between HER2 and MAL2, Ezrin, NHERF1, and PMCA2 in trastuzumab-resistant SKBR3 cells

(A) Immunofluorescence staining for cholera toxin B (lipid rafts) in control and trastuzumab-resistant SKBR3 cells. Scale bars represent 10 μm.

(B) Immunofluorescence staining for HER2 and MAL2 in control and trastuzumab-resistant SKBR3 cells. Scale bars represent 10 μm.

(C) PLA for HER2 and MAL2 in control and trastuzumab-resistant SKBR3 cells also stained for phalloidin. Scale bars represent 10 μm.

(D–F) Quantitative results from immunoprecipitation coupled with data-independent acquisition mass spectrometry (DIA-MS) in control and trastuzumab-resistant SKBR3 cells. (D) The DIA-MS Intensity (log_2) of HER2 and MAL2 proteins from control and trastuzumab-resistant SKBR3 cells. (E) The DIA-MS Intensity (log_2) for all the peptide precursor signals of HER2 in control and resistant cells. (F) The DIA-MS peak groups visualized for quantifying HER2 (VLGSGAFGTVYK) and MAL2 (VTLPAGPDILR). Peaks above and below the middle line denote the MS2 and MS1 ion traces in DIA-MS.

(G) MAL2, Ezrin, and NHERF1 mRNA expression in control and trastuzumab-resistant SKBR3 cells as assessed by quantitative RT-PCR (n = 3).

(H) PLA for HER2 with Ezrin (left), NHERF1 (middle), and PMCA2 (right) in control and trastuzumab-resistant SKBR3 cells also stained for phalloidin. Boxed portions are amplified at right with co-registration of PLA signal and immunofluorescence for actin (phalloidin).

(I) Quantitation of PLA experiment for HER2 in combination with MAL2, Ezrin, NHERF1, or PMCA2 represented as the fluorescent intensity of amplified PLA signals associated with membrane protrusions.

(J) Coimmunoprecipitation for HER2 and HSP90 in control and trastuzumab-resistant SKBR3 cells.

(K) PLA for HER2 and HSP90 in control and trastuzumab-resistant SKBR3 cells also stained for phalloidin. Scale bars represent 10 μm.

(L) XTT cell viability assay in control, MAL2KD-treated, and MβCD-treated trastuzumab-resistant SKBR3 and BT474 cells.

(M) Immunofluorescence staining for FOXO1 in control, MAL2KD-treated, and MβCD-treated trastuzumab-resistant SKBR3 cells.

(N) Immunofluorescence staining for HER2 and pAKT in control, MAL2KD-treated, and MβCD-treated trastuzumab-resistant SKBR3 cells. Scale bars represent 10 μm.

(O) Diagram representing the structure of MAL2- and lipid raft-enriched membrane protrusions containing multi-protein HER2 signaling complexes. These results are representative of three independent experiments.

KEY RESOURCES TABLE

REAGENT or RESOURCE	SOURCE	IDENTIFIER
Antibodies		
ErbB2 (HER-2) Monoclonal Antibody (CB11)	Thermo Fisher Scientific	Cat#MA1-35720: RRID:AB_1073585
MAL2 Polyclonal antibody	Thermo Fisher Scientific	Cat# BS-7175R
Rabbit Anti-NHERF-1 Polyclonal Antibody, Unconjugated, Clone H-100	Santa Cruz Biotechnology	Cat# sc-134485: RRID:AB_2191505
PMCA2 ATPase Polyclonal Antibody	Thermo Fisher Scientific	Cat# PA1-915: RRID:AB_2243199
Ezrin Antibody	Cell Signaling	Cat# 3145: RRID:AB_2100309
EGFR Antibody	Cell Signaling	Cat# 4267
Neu (3B5) antibody	Santa Cruz Biotechnology	Cat# sc-33684: RRID:AB_627996
HSP90 beta Monoclonal Antibody (H9010)	Thermo Fisher Scientific	Cat#37-9400: RRID:AB_2533349
Phospho-HER2/ErbB2 (Tyr1221/1222) (6B12) Rabbit mAb	Cell Signaling	Cat#2243S
EGF Receptor (D38B1) XP® Rabbit mAb	Cell Signaling	Cat#4267S
Akt (pan) (C67E7) Rabbit mAb	Cell Signaling	Cat#4691S
Phospho-Akt (Ser473) (D9E) XP® Rabbit mAb	Cell Signaling	Cat#4060S
p-EGFR Antibody (Tyr 1173)	Santa Cruz Biotechnology	Cat#sc-12351
Flotillin-1 Antibody (H-104)	Santa Cruz Biotechnology	Cat#sc-25506
MAL2 Polyclonal Antibody	Bioss	Cat#BS-7175R
Rabbit Anti-NHERF-1 Polyclonal Antibody, Unconjugated, Clone H-100	Santa Cruz Biotechnology	Cat# sc-134485: RRID:AB_2191505
Anti-HA-Tag Antibody (F-7)	Santa Cruz Biotechnology	Cat# sc-7392
HA-Tag (C29F4) Rabbit mAb	Cell Signaling	Cat#3724S
Anti-OctA-Probe Antibody (H-5)	Santa Cruz Biotechnology	Cat# sc-166355
FKHR (H-128) antibody	Santa Cruz Biotechnology	Cat# sc-11350: RRID:AB_640607
Chemicals, peptides, and recombinant proteins		
β-cyclodextrin(MβCD)	Sigma-Aldrich	Cat# C4555
Wortmannin	Cell Signaling	Cat# 9951s
Ionomycin	Thermo Fisher Scientific	Cat# 124222
Puromicyn	Thermo Fisher Scientific	Cat# A1113803
Human Epidermal Growth Factor (hEGF)	Cell Signaling	Cat# 8916
Cholera Toxin Subunit B (Recombinant), Alexa Fluor™ 555 Conjugate		Cat# C34766
Phalloidin–Atto 665	Sigma-Aldrich	Cat# 04497
Critical commercial assays		
Duolink™ assay kit	Sigma-Aldrich	Cat#DUO94002
SuperScript III Platinum One-Step qRT-PCR Kit	Invitrogen	Cat#74106
Step One Plus Real-Time PCR System	Applied Biosystems	Cat#4376600
ProLong™ Gold Antifade Mountant with DAPI	Thermo Fisher Scientific	Cat# P36941
Deposited data		
Raw and analyzed data	This paper	GEO: GSE188513
Single cell RNA sequencing data	Chung et al., (2017)2017	GEO:GSE75688

REAGENT or RESOURCE	SOURCE	IDENTIFIER
ATAC sequencing data (MCF10A)	(Liu et al., 2017)	GEO: GSE89013
ATAC sequencing data (MCF7)	(Guan et al., 2019)	GEO: GSE117940
ATAC sequencing data (MDA-MD-231)	(Cai et al., 2020)	GEO: GSE129646
Microarray	Jeong et al., (2016)2016	GEO: GSE62555
Experimental models: Cell lines		
Cell line: SK-BR-3	ATCC	Cat# HTB-30, RRID:CVCL_0033
Cell line: BT-474	ATCC	Cat# CRL-7913, RRID:CVCL_0179
Oligonucleotides		
TaqMan Hs00195134_m1, flotillin1	Thermo Fisher Scientific	Cat#4331182
TaqMan Hs00707014_s1, MAL	Thermo Fisher Scientific	Cat#4331182
TaqMan Hs01043579_u1, MAL2	Thermo Fisher Scientific	Cat#4351372
TaqMan Hs01090447_m1, PMCA2	Thermo Fisher Scientific	Cat#4331182
TaqMan Hs00931646_m1, Ezrin	Thermo Fisher Scientific	Cat#4331182
TaqMan Hs00188594_m1, NHERF1	Thermo Fisher Scientific	Cat#4331182
Human HPRT1 (HGPRT) Endogenous Control (VIC™/MGB probe, primer limited)	Applied Biosystems	Cat#4326321E
Recombinant DNA		
Flotillin 1 (FLOT1) (NM_005803) Human Tagged ORF Clone	Origene	Cat#RC200231
MAL2 (NM_052886) Human Tagged ORF Clone	Origene	Cat#RC203862
GFP-C1-PLCdelta-PH	Addgene	Cat#21179
pN1-Lck-GCaMP5G	Addgene	Cat#34924
Software and algorithms		
Step One Software v2.2.2	Applied Biosystems	N/A
GraphPad Prism 6.0	GraphPad Software	RRID:SCR_002798
ZEN Digital Imaging Light Microscopy	Zeiss	RRID:SCR_013672
Zen 2012 SP2 software	Zeiss	N/A
Bruker MS FX PRO software	Bruker	RRID:SCR_017365
Spectronaut v13	Biognosys	N/A
IPA 48207413	QIAGEN	RRID:SCR_008653
DESeq v2	Bioconductor	RRID:SCR_000154
StringTie v2.0	(Pertea et al., 2015)	https://ccb.jhu.edu/software/stringtie/
Seurat v3.1.0	(Butler et al., 2018)	https://satijalab.org/seurat/
Cutadapt	(Martin, 2011)	https://cutadapt.readthedocs.io/en/stable/
Bowtie2	(Langmead and Salzberg, 2012)	http://bowtie-bio.sourceforge.net/bowtie2/index.shtml
Samtools	(Li et al., 2009)	http://samtools.sourceforge.net/
Picard	http://broadinstitute.github.io/picard/	https://broadinstitute.github.io/picard/
deepTools	(Ramírez et al., 2016)	https://deeptools.readthedocs.io/en/develop/
HOMER	(Heinz et al., 2010)	http://homer.ucsd.edu/homer/
Integrative Genomics Viewer (IGV)	(Robinson et al., 2011)	https://software.broadinstitute.org/software/igv/
Other		

REAGENT or RESOURCE	SOURCE	IDENTIFIER
8-well Chamber Slide w/removable wells	Thermo Fisher Scientific	Cat# 154534PK